INTERNATIONAL JOURNAL FOR NUMERICAL METHODS IN FLUIDS, VOL. 9, 43–57 (1989)

VELOCITY–PRESSURE INTEGRATED VERSUS PENALTY FINITE ELEMENT METHODS FOR HIGH-REYNOLDS-NUMBER FLOWS

S.-W. KIM* AND RAND A. DECKER†

Fluid Dynamics Branch, NASA-MSFC/ED 42, Huntsville, Alabama 35812, U.S.A.

SUMMARY

Velocity–pressure integrated and consistent penalty finite element computations of high-Reynolds-number laminar flows are presented. In both methods the pressure has been interpolated using linear shape functions for a triangular element which is contained inside the biquadratic flow element. It has been shown previously that the pressure interpolation method, when used in conjunction with the velocity–pressure integrated method, yields accurate computational results for high-Reynolds-number flows. It is shown in this paper that use of the same pressure interpolation method in the consistent penalty finite element method yields computational results which are comparable to those of the velocity–pressure integrated method for both the velocity and the pressure fields. Accuracy of the two finite element methods has been demonstrated by comparing the computational results with available experimental data and/or fine grid finite difference computational results. Advantages and disadvantages of the two finite element methods are discussed on the basis of accuracy and convergence nature. Example problems considered include a lid-driven cavity flow of Reynolds number 10 000, a laminar backward-facing step flow and a laminar flow through a nest of cylinders.

KEY WORDS Finite element Penalty method Consistent penalty

INTRODUCTION

Various finite element methods for the Navier–Stokes equations have been proposed during the last decades. These finite element methods may be categorized into three classes based on the way pressure has been treated: velocity–pressure integrated mixed interpolation methods,[1–3] penalty methods[3–5] and velocity–pressure segregated methods.[6–8]

The velocity–pressure integrated mixed interpolation methods do not require any approximation at the differential equation level, whereas simplified pressure and/or pressure correction equations are used in the velocity–pressure segregated methods, and the penalized conservation of mass equation is used in the penalty methods. Conceptually, the velocity–pressure integrated methods would satisfy the conservation of mass equation most rigorously. An eight-node velocity, four-node pressure flow element has been used most frequently in the early development stage of the finite element method for flows.[1] Unfortunately, this element yielded inaccurate pressure as the Reynolds number was increased.[9] A compilation of various flow elements which yielded improved pressure can be found in Reference 9, among many others. However, high-Reynolds-number flows

* Present address: ICOMP, MS 5-3, NASA Lewis Research Center, 21000 Brookpark Road, Cleveland, OH 44135, U.S.A.
† NRC Research Associate.

0271–2091/89/010043–15$07.50

Received 5 October 1987
Revised 3 April 1988

(i.e. cavity flow for a Reynolds number of 10000) have seldom been considered except in References 2 and 10. In References 2 and 4 a nine-node velocity, three-node pressure flow element was introduced; it was shown that this flow element, when used in the velocity–pressure integrated finite element method, yielded accurate computational results for high-Reynolds-number flows.

The velocity–pressure segregated methods have been motivated by the success of the finite difference computational methods based on segregated formulation of the Navier–Stokes equations, such as the SIMPLE (semi-implicit method for pressure-linked equations) algorithm.[11] In the segregated methods significant computational efficiency can be achieved in computer storage and computational time compared with the other two classes of methods.

In the penalty method the pressure variable is pre-eliminated from the Navier–Stokes equations by penalizing the conservation of mass equation. The conservation of mass constraint can be satisfied rigorously as the penalty number approaches infinity. The influence of the penalty number on the converged solution can be found in Reference 12, among many others. The consistent penalty method studied in this paper is the same as that of Reference 4 except that a new pressure interpolation method has been used. The improvements realized by introducing the new pressure interpolation polynomial into the consistent penalty method are also discussed in detail. It is shown that the penalty method and the velocity–pressure integrated method yield comparable computational results for both the velocity and the pressure fields in terms of accuracy and convergence rate.

The example problems were solved using a frontal solver and the direct (Picard) iteration method.[1, 13] Inclusion of the Newton–Raphson method into the present finite element code[14] has not been considered, since computation of turbulent flows usually requires the most strongly convergent solution technique, which may require severe under-relaxation to obtain convergent solutions.[15–17]

FINITE ELEMENT EQUATIONS

A finite element system of equations for two-dimensional, laminar, steady, incompressible flows is described below. The method is based on the standard Galerkin finite element method.[1] In the following discussions consistent notations are used throughout, and repeated indices imply summation over the indices unless otherwise specified.

The Navier–Stokes equations are given as

$$\left.\begin{aligned} \rho u_j \frac{\partial u_i}{\partial x_j} - \frac{\partial}{\partial x_j}\left[\mu\left(\frac{\partial u_i}{\partial x_j}+\frac{\partial u_j}{\partial x_i}\right)-p\delta_{ij}\right] &= b_i \qquad (1)\\ \frac{\partial u_j}{\partial x_j} &= 0 \qquad (2)\end{aligned}\right\} \text{ in } \Omega,$$

where Ω is the open bounded domain, the subscripts i and j denote co-ordinate directions, ρ is the density of the fluid, u_i is the velocity component in the ith co-ordinate direction, p is the pressure, μ is the molecular viscosity of the fluid, b_i is the body force in the ith co-ordinate direction and δ_{ij} is the Kronecker delta such that $\delta_{ij}=1$ for $i=j$ and $\delta_{ij}=0$ for $i\neq j$. The boundary conditions used are given as

$$\begin{aligned} \mathbf{u} &= \mathbf{u}_0(\mathbf{x}) \qquad \text{for } \mathbf{x}\in\partial\Omega_1,\\ T_i &= \tau_{ij}n_j \qquad \text{for } \mathbf{x}\in\partial\Omega_2, \end{aligned} \qquad (3)$$

where $\mathbf{x}=(x, y)$, $\partial\Omega_1$ is part of the boundary on which a Dirichlet boundary condition is specified, $\partial\Omega_2$ is the rest of the boundary on which natural boundary conditions are specified, T_i is the surface traction and τ_{ij} is the stress tensor given as $\tau_{ij}=\mu(\partial u_i/\partial x_j+\partial u_j/\partial x_i)-p\delta_{ij}$.

In the penalty method the conservation of mass equation is expressed as

$$\frac{\partial u_j}{\partial x_j}=-\frac{1}{\lambda}p, \tag{4}$$

where λ is the penalty number.

The finite element system of equations for the penalty method is given below. Detailed derivation of the finite element system of equations can be found in References 1, 2 and 10, among many others. The system of equations for an element (Ω_e) is given in matrix form as

$$\begin{bmatrix}\mathbf{C} & \mathbf{0}\\ (\text{sym}) & \mathbf{C}\end{bmatrix}+\begin{bmatrix}\mathbf{K}_0 & \mathbf{0}\\ (\text{sym}) & \mathbf{K}_0\end{bmatrix}+\begin{bmatrix}\mathbf{K}_{11} & \mathbf{K}_{12}\\ \mathbf{K}_{21} & \mathbf{K}_{22}\end{bmatrix}\begin{Bmatrix}\mathbf{u}_1\\ \mathbf{u}_2\end{Bmatrix}-\begin{bmatrix}\mathbf{Q}_1\\ \mathbf{Q}_2\end{bmatrix}\{\mathbf{p}\}=\begin{Bmatrix}\mathbf{f}_1\\ \mathbf{f}_2\end{Bmatrix}+\{\text{b.c.}\}, \tag{5}$$

$$[\mathbf{Q}_1^{\mathrm{T}}\ \mathbf{Q}_2^{\mathrm{T}}]\begin{Bmatrix}\mathbf{u}_1\\ \mathbf{u}_2\end{Bmatrix}=-\frac{1}{\lambda}[\mathbf{M}_p], \tag{6}$$

where

$$\mathbf{C}=\int_{\Omega_e}\boldsymbol{\phi}^{\mathrm{T}}\rho(\mathbf{u}_j^{\mathrm{T}}\boldsymbol{\phi})\frac{\partial\boldsymbol{\phi}}{\partial x_j}\,\mathrm{d}\mathbf{x}, \tag{7}$$

$$\mathbf{K}_0=\int_{\Omega_e}\frac{\partial\boldsymbol{\phi}^{\mathrm{T}}}{\partial x_j}\mu\frac{\partial\boldsymbol{\phi}}{\partial x_j}\,\mathrm{d}\mathbf{x}, \tag{8}$$

$$\mathbf{K}_{ij}=\int_{\Omega_e}\frac{\partial\boldsymbol{\phi}^{\mathrm{T}}}{\partial x_j}\mu\frac{\partial\boldsymbol{\phi}}{\partial x_i}\,\mathrm{d}\mathbf{x}, \tag{9}$$

$$\mathbf{Q}_i=\int_{\Omega_e}\frac{\partial\boldsymbol{\phi}^{\mathrm{T}}}{\partial x_i}\boldsymbol{\psi}\,\mathrm{d}\mathbf{x}, \tag{10}$$

$$\mathbf{f}_i=\int_{\Omega_e}\boldsymbol{\phi}^{\mathrm{T}}b_i\,\mathrm{d}\mathbf{x}, \tag{11}$$

$$\mathbf{M}_p=\int_{\Omega_e}\boldsymbol{\psi}^{\mathrm{T}}\boldsymbol{\psi}\,\mathrm{d}\mathbf{x}, \tag{12}$$

$\mathbf{u}_i$ is a column vector of nodal values of the velocity component u_i, $\mathbf{p}$ is a column vector of nodal pressure, $\boldsymbol{\phi}$ is a column vector of interpolating polynomials for velocity, $\boldsymbol{\psi}$ is a column vector of interpolating polynomials for pressure, {b.c.} is a column vector contributed by the specified flux boundary condition and the subscripts i and j denote the spatial dimensions. Equations (7)–(12) have been integrated using the Gauss numerical quadrature method with three Gauss points in each co-ordinate direction.

For the velocity–pressure integrated case the element system of equations given as equations (5) and (6), with the right-hand side of equation (6) replaced by a null column vector, have been assembled to obtain the global system of equations. In the penalty finite element method equation (6) has been inverted to obtain a column vector of the nodal pressure and the result has been

substituted into equation (5) to obtain

$$\begin{bmatrix} \mathbf{C} & \mathbf{0} \\ (\text{sym}) & \mathbf{C} \end{bmatrix} + \begin{bmatrix} \mathbf{K}_0 & \mathbf{0} \\ (\text{sym}) & \mathbf{K}_0 \end{bmatrix} + \begin{bmatrix} \mathbf{K}_{11} & \mathbf{K}_{12} \\ \mathbf{K}_{21} & \mathbf{K}_{22} \end{bmatrix} \begin{Bmatrix} \mathbf{u}_1 \\ \mathbf{u}_2 \end{Bmatrix} + \lambda \begin{bmatrix} \mathbf{Q}_1 \\ \mathbf{Q}_2 \end{bmatrix} [\mathbf{M}_p] [\mathbf{Q}_1^T \, \mathbf{Q}_2^T] \begin{Bmatrix} \mathbf{u}_1 \\ \mathbf{u}_2 \end{Bmatrix} = \begin{Bmatrix} \mathbf{f}_1 \\ \mathbf{f}_2 \end{Bmatrix} + \{\text{b.c.}\}. \tag{13}$$

The flow element is described below. The velocities were interpolated using the biquadratic shape functions and the pressure was interpolated using the linear shape functions defined on a triangular element which is contained inside the quadratic element; see Figure 1. The three pressure nodes are located at the three Gauss points of the three-point Gauss quadrature rule for quadrilateral elements.[18] The co-ordinates of the pressure nodes on the computational element are given as[2]

$$\xi_n = \begin{cases} (0, \sqrt{2}/\sqrt{3}) & \text{for } n=1, \\ (1/\sqrt{2}, -1/\sqrt{6}) & \text{for } n=2, \\ (1/\sqrt{2}, -1/\sqrt{6}) & \text{for } n=3, \end{cases} \tag{14}$$

where $\xi_n = (\xi_n, \eta_n)$ and n denotes the pressure node numbers. The shape functions for each of the nodes are given as

$$\begin{aligned} \psi_1 &= \frac{1}{3} + \frac{\sqrt{2}}{\sqrt{3}}\eta, \\ \psi_2 &= \frac{1}{3} - \frac{1}{\sqrt{2}}\xi - \frac{1}{\sqrt{6}}\eta, \\ \psi_3 &= \frac{1}{3} + \frac{1}{\sqrt{2}}\xi - \frac{1}{\sqrt{6}}\eta. \end{aligned} \tag{15}$$

The other pressure interpolation polynomials studied are given as[4]

$$\boldsymbol{\psi}^T = \{1, x, y\} \tag{16}$$

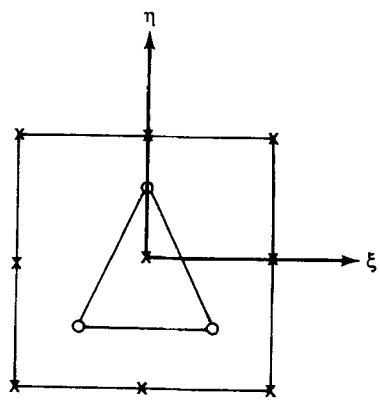

Figure 1. A nine-node velocity, three-node pressure flow element: ×, velocity node; ○, pressure node

and

$$\psi^{\mathrm{T}} = \{1, \xi, \eta\}. \tag{17}$$

The three pressure interpolation methods given as equations (15)–(17) belong to the same approximation space when rectangular elements are used, but only equations (15) and (17) belong to the same approximation space when non-rectangular elements are used. Thus any difference between the computational results obtained by using the pressure interpolation polynomials which belong to the same approximation space should be related to the computer round-off error and the matrix condition.[13] The performances of these three pressure interpolation polynomials are discussed in terms of numerical stability and convergence rate in the following section.

The assembled global system of equations was solved by a direct (Picard) iteration method using a frontal solver, and the solutions were updated using an under-relaxation method given as

$$a_j^* = \alpha a_j^n + (1-\alpha) a_j^{n-1}, \tag{18}$$

where a_j represents any degree of freedom, α is the under-relaxation number, the superscripts n and $n-1$ denote the iteration levels and a_j^* is the updated solution. No under-relaxation was necessary for low-Reynolds-number flows. However, $\alpha = 0{\cdot}8$ and $\alpha = 1$ have been used for velocities and pressure respectively to obtain convergent solutions for high-Reynolds-number flows (i.e. cavity flow at a Reynolds number of 10000). With use of these under-relaxation parameters, divergent and/or convergent to non-physical solutions have not been encountered for all the example flows considered herein.

EXAMPLE PROBLEMS

The finite element methods described in the previous section were tested by solving a lid-driven cavity flow,[10, 12, 19–21] a laminar backward-facing step flow[22, 23] and a laminar flow through a nest of cylinders.[24–26] For cavity flow at a Reynolds number of 10000, sharp boundary layers develop along all the boundary edges of the cavity. For the backward-facing step flow, the flow has to expand abruptly at the convex corner of the backward-facing step and a strong pressure gradient is formed at the same corner. Owing to these facts, obtaining convergent solutions with any iterative numerical method can be quite difficult.[23] Therefore these two flows provide serious test cases for any numerical method. To further investigate the convergence nature of the pressure interpolation methods for arbitrary distorted quadrilateral elements, a laminar flow through a nest of cylinders has also been included in this paper.

In the following discussion, solving the coupled system of equations once is counted as an iteration. The convergence rate versus the number of iterations is discussed based on the error criterion (ε) defined as

$$\varepsilon = \max_{j=1,T} (|1 - a_j^n / a_{\max}^n|), \tag{19}$$

where a_j denotes a nodal value of velocity component or pressure; $a_{\max}$ denotes the maximum velocity in the flow domain if a_j is the velocity degree of freedom, and denotes the maximum pressure if a_j is the pressure degree of freedom; and T is the total number of degrees of freedom.

In non-linear problems the required number of iterations to obtain a convergent solution depends on the prescribed convergence criterion. In the penalty method the pressure is recovered from the converged velocity solution in the post-process, and the quality of the recovered pressure depends on the velocity. In order to track down the convergence history of the pressure, the pressure was recovered at the end of each iteration in the present study. The purpose was to

provide some insight into the convergence nature of the penalty methods, which would be helpful in deciding the convergence criterion for velocity in application situations. For the penalty methods a penalty number of $(\mu/\rho)\times 10^{10}$ has been used.

The pressure is discontinuous across element boundaries. Thus the nodal pressure at the velocity node has been obtained by averaging all the pressure contributions made by the elements containing the node; and each of the contributions was computed using equations (15)–(17), respectively.

For convenience in the following discussion, the velocity–pressure integrated method with the pressure interpolation polynomials given as equation (15) is denoted as the VP-INT method, and the consistent penalty method with the pressure interpolation polynomials given as equations (15)–(17) is denoted as the PNLT-K, PNLT-E and PNLT-D methods respectively.

Lid-driven cavity flow

A lid-driven cavity flow for a Reynolds number of 10000 is considered below. Fine grid finite difference computational results for the same flow can be found in References 20 and 21. The no-slip boundary condition ($u=v=0$) has been prescribed at all the boundaries except $y=1$, where $u=1$ and $v=0$. For the VP-INT method a fixed pressure boundary condition was specified at an arbitrary pressure node inside the flow domain. The Reynolds number is defined as $R_e=\rho UL/\mu$, where $U=1$ is the velocity of the lid, $L=1$ is the reference length, ρ is the density and μ is the molecular viscosity of the fluid. The computational domain was discretized by unequally spaced 32×32 quadratic elements.[2] The trivial solution ($u=v=p=0$) was used as an initial guess for the Reynolds number of 10000, for all the cases.

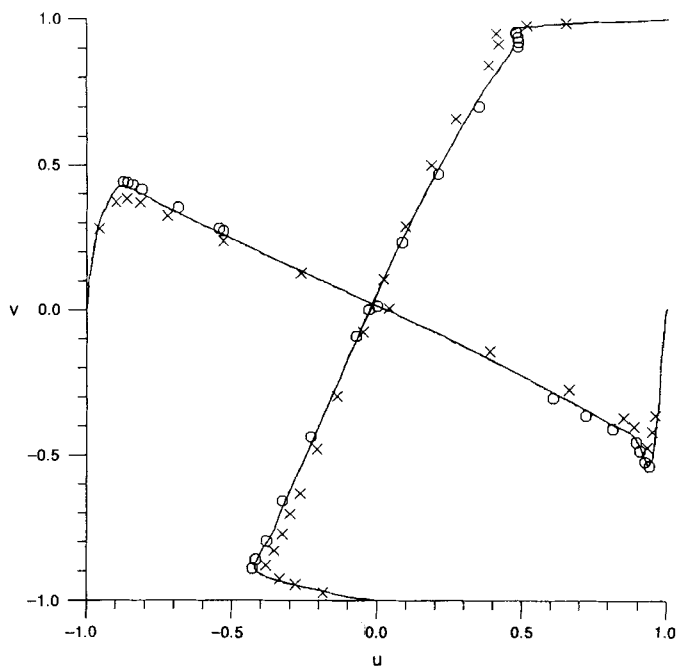

Figure 2. Horizontal and vertical velocity profiles for cavity flow at Reynolds number of 10000: ———, VP-INT method; — — —, PNLT-K method; --------, PNLT-E method; — · —, PNLT-D method

The horizontal velocity profiles at $x=0{\cdot}5$ and the vertical velocity profiles at $y=0{\cdot}5$ are compared with those of Ghia *et al.*[20] and Schreiber and Keller[21] in Figure 2. It can be seen that the four methods yielded almost identical velocity profiles and that the present computational results compare more favourably with those of Ghia *et al.*[20] than with those of Schreiber and Keller.[21] Comparison of the horizontal velocity profiles obtained by the VP-INT method with those of Ghia *et al.*[20] and Schreiber and Keller[21] for various Reynolds numbers can be found in Reference 2, where it can be seen that the finite element computational results compared favourably with those of the cited references.

The streamline and normalized pressure contours obtained by using the PNLT-K and PNLT-E methods are shown in Figures 3 and 4 respectively. The normalized pressure P was obtained from the computed static pressure p using $P=pL/U/\mu$.[19] The streamline and pressure contour labels are given in Table I. The streamline and pressure contours obtained by using the VP-INT and PNLT-D methods were almost identical to those shown in Figure 3. The pressure contour obtained by using the PNLT-E method exhibited a few distorted pressure contour lines at the top region of the cavity; see Figure 4(b). It was found that the distorted pressure contour lines were caused by the

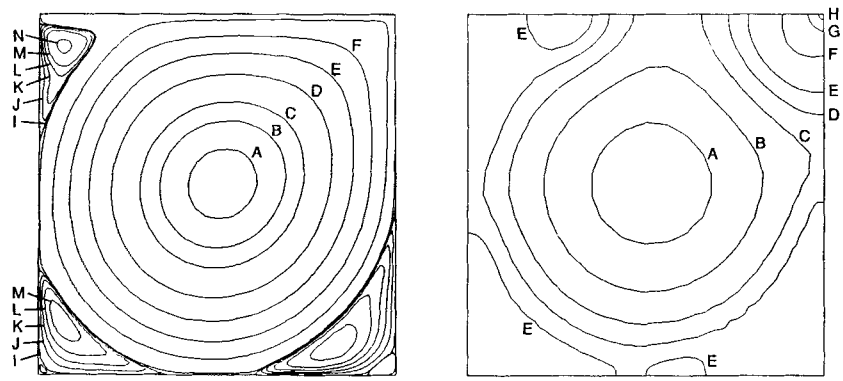

Figure 3. Cavity flow for $Re=10000$, PNLT-K method: (a) streamline; (b) pressure

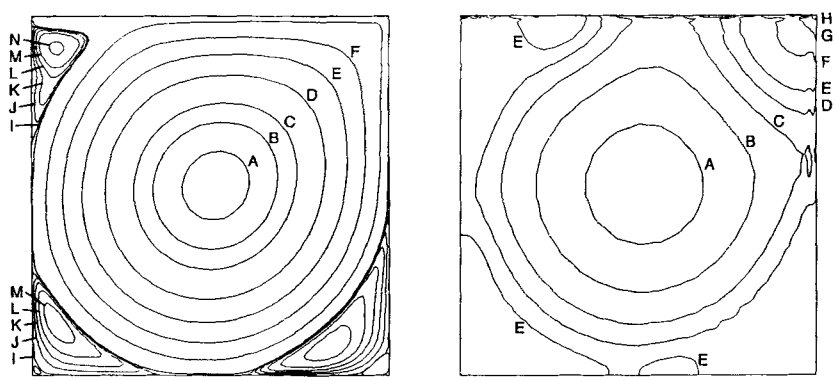

Figure 4. Cavity flow for $Re=10000$, PNLT-E method: (a) streamline; (b) pressure

Table I. Contour labels for cavity flow

(a) Streamline contour

Label	ψ	Label	ψ	Label	ψ
A	−0·11	F	−0·03	K	2×10^{-4}
B	−0·10	G	−0·01	L	5×10^{-4}
C	−0·09	H	-1×10^{-10}	M	1×10^{-3}
D	−0·07	I	1×10^{-6}	N	2×10^{-3}
E	−0·05	J	5×10^{-5}		

(b) Pressure contour

Label	P	Label	P	Label	P
A	−900	D	−200	G	1000
B	−650	E	0	H	3000
C	−400	F	400		

pressure matrix $\mathbf{M}_p$ and the coefficients of the pressure interpolation polynomials. The entries of the pressure matrix $\mathbf{M}_p$ were different by several orders of magnitude, and the coefficients of the pressure interpolation polynomials, i.e. the coefficients for $(1, x, y)$, were about ten orders of magnitude different for the high-aspect-ratio fine grids located along the boundary of the cavity. However, these distorted pressure contour lines may disappear if a different pressure-averaging technique is used. An alternative pressure-averaging technique is discussed in the section 'Flow through a nest of cylinders'.

The error norm versus the number of iterations for each flow variable is shown in Figure 5. It can be seen that the VP-INT method yielded a uniformly convergent solution for the relative error as small as 10^{-7}. The PNLT-K and PNLT-D methods exhibited convergence rates comparable with that of the VP-INT method. On the other hand, the PNLT-E method exhibited poorer convergence behaviour than the other methods. Again, the ill conditioned pressure matrix $\mathbf{M}_p$ and the computer round-off error were responsible for the degenerated convergence rate of the PNLT-E method. For all the cases, practically convergent solutions (i.e. $\varepsilon \approx 1\times10^{-4}$) were obtained after 35 iterations.

In general, the present finite element computational results obtained by using the 32×32 quadratic elements (or equivalently, a 65×65 mesh) compared favourably with those of Ghia *et al.*,[20] in which 129×129 and 257×257 meshes were used, and with those of Schreiber and Keller,[21] in which a 180×180 mesh was used, for the same Reynolds number of 10000.

Backward-facing step flow

A laminar backward-facing step flow is considered below. The experimental data can be found in Armaly *et al.*[22] In the following discussion, the Reynolds number $Re=\rho VD/\mu$ is based on the hydraulic diameter ($D=0{\cdot}0104$ m) and the bulk velocity ($V=0{\cdot}6667\ \mathrm{m\,s^{-1}}$) at the inlet. The experimental data show that there exists only one recirculation zone at the downstream region of the backward-facing step for a Reynolds number less than approximately 450, and that a second recirculation zone appears at the top wall of the channel for Reynolds numbers of approximately 450 and beyond. A Reynolds number of 500 has been considered in this paper. A complete set of computational results obtained by using the velocity–pressure integrated method for Reynolds

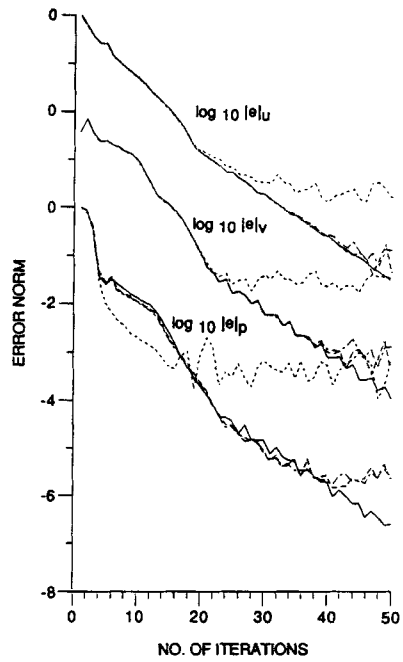

Figure 5. Error norm versus number of iterations for cavity flow: ———, VP-INT method; — — —, PNLT-K method; --------, PNLT-E method; ———, PNLT-D method

numbers of 10–900 can be found in Reference 2, and a finite difference computation of the same backward-facing step flow can be found in Kim and Moin,[23] among many others.

The inlet boundary is located at 3 step heights upstream of the step, and the exit boundary at 45 step heights downstream of the step. The computational domain was discretized by 44×15 quadratic elements (or equivalently, an 89×31 mesh) in the flow direction and transverse direction respectively. The velocity profile of a fully developed channel flow was used as the inlet boundary condition. Vanishing normal stress was prescribed at the exit boundary. For the VP-INT method a fixed pressure boundary condition cannot be prescribed together with the vanishing normal stress boundary condition.[27] The trivial solution ($u=v=p=0$) was used as an initial guess.

The streamline and pressure contours obtained by using the PNLT-K and PNLT-E methods are shown in Figures 6 and 7 respectively. The pressure has been normalized using $P=pL_{\text{ref}}/V_{\text{ref}}/\mu$, where $L_{\text{ref}}=0{\cdot}0049$ m is the step height and V_{ref} is the bulk velocity at the inlet. The labels for the streamline and pressure contours are given in Table II. The streamline and pressure contours obtained by using the VP-INT and PNLT-D methods were identical to those shown in Figure 6. The PNLT-E method yielded the similar distorted pressure contour lines in the downstream region of the channel for the same reasons discussed previously; see Figure 7.

The error norm versus the number of iterations for each flow variable is shown in Figure 8. Practically convergent solutions were obtained after approximately 50 iterations for all the cases. The VP-INT method yielded a uniformly convergent solution as before. The PNLT-K, PNLT-E and PNLT-D methods yielded rapidly convergent solutions as for the VP-INT method at earlier iterations. As the number of iterations was increased, the PNLT-E method yielded an oscillatory solution for the same reasons discussed in the previous cavity flow example.

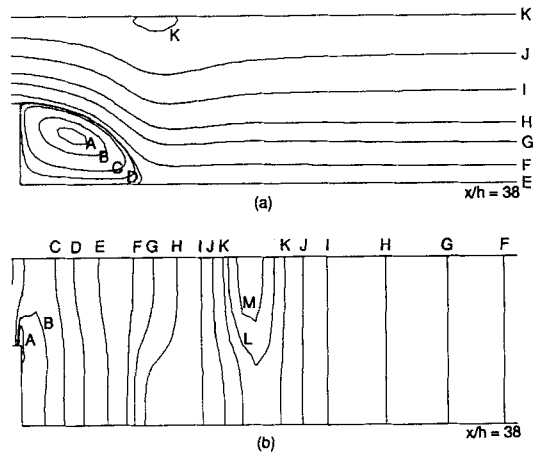

Figure 6. Backward-facing step flow, PNLT-K method: (a) streamline; (b) pressure

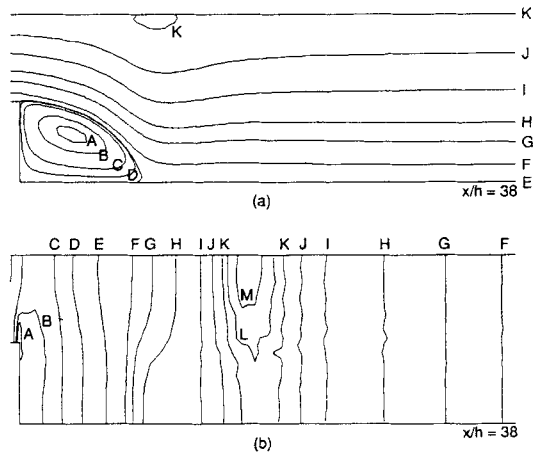

Figure 7. Backward-facing step flow, PNLT-E method: (a) streamline; (b) pressure

The present computational results compared favourably with the experimental data as well as with the fine grid finite difference computational results of Kim and Moin,[23] in which a 101×101 grid was used.

Flow through a nest of cylinders

Flows through a nest of cylinders can be found in a number of engineering applications, such as the Space Shuttle main engine–main injector assembly (SSME–MIA) and the heat exchangers in nuclear reactors; see Reference 24 for more details. However, these flows began to be solved numerically only very recently. The solutions involved a finite element computation of a two-dimensional laminar flow through a nest of cylinders[25] and a body-fitted grid finite difference computation of a three-dimensional laminar flow through a nest of cylinders.[26] Neither experimental data nor detailed computational results are available for these flows as yet.

Table II. Contour labels for backward-facing step flow

(a) Streamline contour

Label	ψ	Label	ψ	Label	ψ
A	$-2{\cdot}0\times10^{-4}$	F	$1{\cdot}0\times10^{-4}$	K	$3{\cdot}467\times10^{-3}$
B	$-1{\cdot}5\times10^{-4}$	G	$5{\cdot}0\times10^{-4}$	L	$3{\cdot}480\times10^{-3}$
C	$-5{\cdot}0\times10^{-5}$	H	$1{\cdot}0\times10^{-3}$	M	$3{\cdot}50\times10^{-3}$
D	$-1{\cdot}0\times10^{-5}$	I	$2{\cdot}0\times10^{-3}$		
E	0	J	$3{\cdot}0\times10^{-3}$		

(b) Pressure contour

Label	P	Label	P	Label	P
A	−25·5	F	10·0	K	28·5
B	−23·0	G	15·0	L	29·5
C	−18·0	H	20·0	M	29·8
D	−8·0	I	25·0	N	30·0
E	0·0	J	27·0		

Table III. Streamline contour labels for flow through a nest of cylinders

Label	ψ	Label	ψ	Label	ψ
A	−0·04	D	0·4	G	1·0
B	0·0	E	0·6		
C	0·2	F	0·8		

A laminar flow through a nest of cylinders at a Reynolds number of 40 is considered below; see Figure 9. The Reynolds number is defined as $Re=\rho UD/\mu$, where $U=1$ is the free-stream velocity and $D=1$ is the diameter of a cylinder. The inlet boundary was located at 3 diameters upstream of the forward stagnation point of the first column of cylinders, and the exit boundary at 41 diameters downstream of the inlet boundary. A uniform velocity profile was used as the inlet boundary condition. The vanishing normal stress boundary condition was prescribed at the exit boundary, and the symmetry boundary condition at the top and bottom of the computational domain. The computational domain was discretized by 1024 quadratic elements with 4369 nodes. The finite element mesh in the vicinity of the nest of cylinders is shown in Figure 9. The trivial solution ($u=v=p=0$) was used as an initial guess.

The streamline and pressure contours obtained by using the PNLT-K and PNLT-E methods are shown in Figures 10 and 11 respectively. The pressure has been normalized using $P=p/(\rho U^2/2)$, where $U=1$ is the reference velocity at the inlet boundary. An arbitrary reference pressure ($p=0{\cdot}0$) has been assigned at the forward stagnation point of the first column of cylinders. The streamline contour labels are given in Table III. In Figures 10 and 11 the minimum and maximum normalized pressures P are $-20{\cdot}0$ and $0{\cdot}0$ respectively; and the incremental normalized pressure ΔP between the contour lines is $1{\cdot}0$. The streamline and pressure contours obtained by using the VP-INT and PNLT-D methods were identical to those shown in Figure 10. The PNLT-E method yielded severely distorted pressure contour lines for the same reasons listed previously;

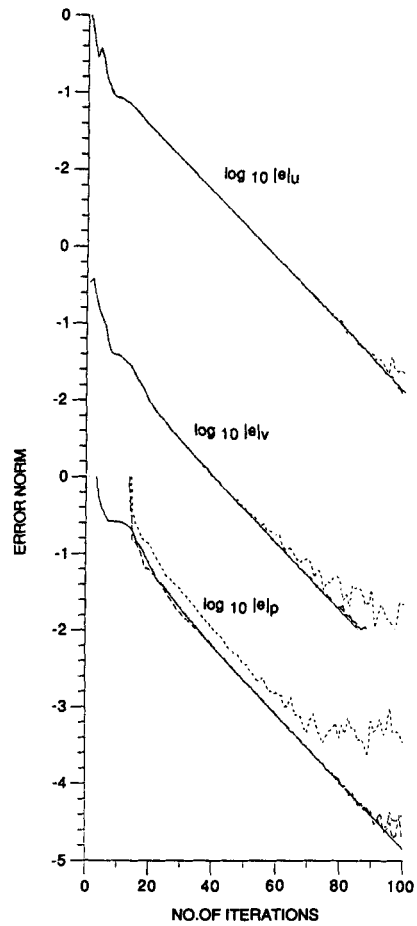

Figure 8. Error norm versus number of iterations for backward-facing step flow: ———, VP-INT method; – – –, PNLT-K method; --------, PNLT-E method; — — —, PNLT-D method

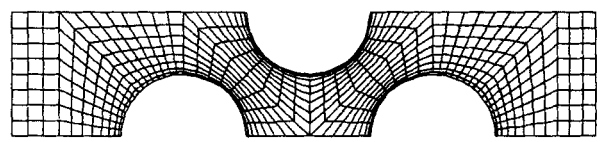

Figure 9. Flow through a nest of cylinders; grid in the vicinity of the nest of cylinders

see Figure 11. An alternative pressure-averaging technique would be to compute the pressure at the centre (i.e. $\xi = \eta = 0$) of the quadrilateral element and to use an area-weighted average to obtain the nodal pressure. However, this alternative pressure-averaging technique has not been pursued in the present study for the following two reasons. Firstly, this technique is inconsistent with the present pressure interpolation methods which assume a planar variation of the pressure inside each element. Secondly, all the methods, except the PNLT-E method, yielded clean, smooth pressure contours.

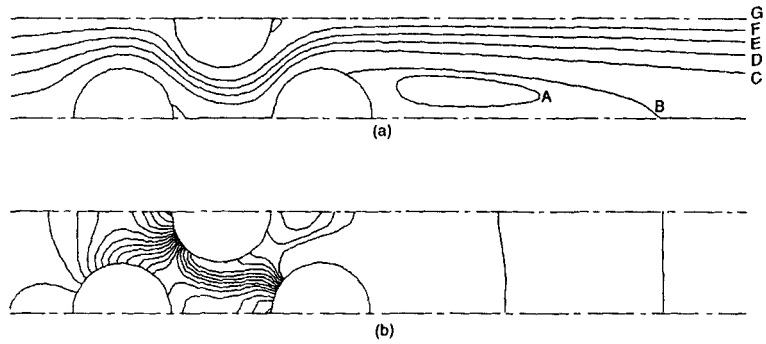

Figure 10. Flow through a nest of cylinders, PNLT-K method: (a) streamline; (b) pressure

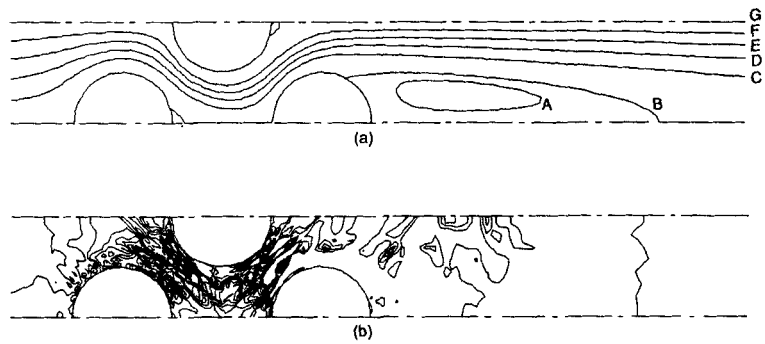

Figure 11. Flow through a nest of cylinders, PNLT-E method: (a) streamline; (b) pressure

The error norm versus the number of iterations for each flow variable is shown in Figure 12. Practically convergent solutions were obtained after approximately 15 iterations for all the cases. The VP-INT method yielded a uniformly convergent solution as before. The PNLT-K, PNLT-E and PNLT-D methods yielded rapidly convergent solutions as the VP-INT method at earlier iterations. For the arbitrary distorted quadrilateral elements with high aspect ratio, the adverse effect of the ill conditioned pressure matrix and the computer round-off error became so severe that only the VP-INT method yielded uniformly convergent pressure as the number of iterations was increased.

CONCLUSIONS AND DISCUSSION

A comparative study of the velocity–pressure integrated and penalty finite element methods has been provided. It has been shown that both the velocity–pressure integrated method and the consistent penalty method yielded accurate computational results for high-Reynolds-number flows. The two finite element methods exhibited almost identical convergence rates for the example problems considered. The penalty method with the pressure interpolation polynomials given in equations (15) and (17) was found to be numerically more stable and yielded a more uniformly convergent solution than that with the pressure interpolation polynomials given in equation (16).

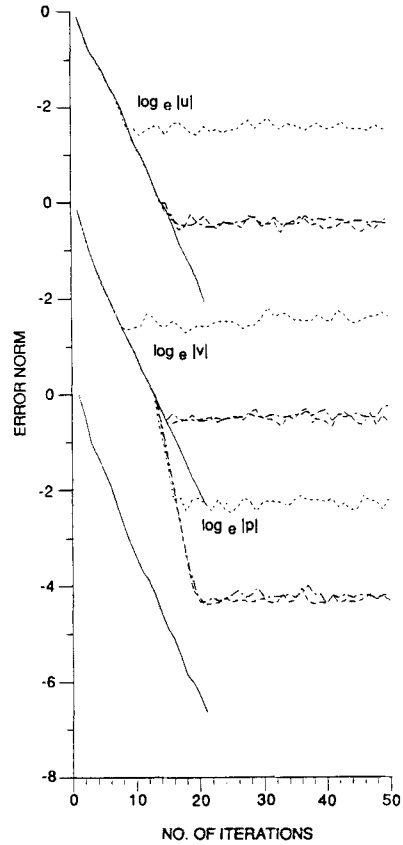

Figure 12. Error norm versus number of iterations for flow through a nest of cylinders: ——, VP-INT method; — — —, PNLT-K method; --------, PNLT-E method; — — —, PNLT-D method

The velocity–pressure integrated and penalty methods yielded almost identical computational results. If the pressure is not the primary concern in application situations, then the penalty method may be more advantageous over the velocity–pressure integrated method since a slight improvement in computational efficiency can be achieved by excluding the conservation of mass equation from the system of equations. For internal flows, for which pressure may be the most important design parameter in many applications, the velocity–pressure integrated method would be preferable to the penalty method because of its uniform convergence behaviour for pressure, especially when arbitrary distorted quadrilateral elements have to be used.

For the example problems considered herein, a relatively small number of grid points, compared with the fine grid finite difference computations of the same example flows, was required to resolve the details of the flow field and to suppress the numerical wiggles without the use of any upwinding technique. The present computational results compared favourably with available experimental data and/or fine grid finite difference computational results.

ACKNOWLEDGEMENT

This work has been supported in part by NASA contract NAS8-35918.

REFERENCES

1. C. Taylor and T. G. Hughes, *Finite Element Programming of the Navier–Stokes Equation*, Pineridge Press, Swansea, 1980.
2. S.-W. Kim, 'A fine grid finite element computation of two-dimensional high Reynolds number flows', *Comput. Fluids*, to appear; also available as *NASA CR-179135*, 1987.
3. O. C. Zienkiewicz, R. L. Taylor and J. M. W. Baynham, 'Mixed and irreducible formulations in finite element analysis', in S. N. Atluri *et al.* (eds), *Hybrid and Mixed Finite Element Methods*, Wiley, New York, 1983.
4. M. S. Engelman, R. L. Sani, P. M. Gresho and M. Bercovier, 'Consistent vs. reduced integration penalty methods for incompressible media using several old and new elements', *Int. j. numer. methods fluids*, **2**, 25–42 (1982).
5. N. Kikuchi, J. T. Oden and Y. J. Song, 'Convergence of modified penalty methods and smoothing schemes of pressure for Stokes' flow problems', in R. H. Gallagher, *et al.* (eds), *Finite Elements in Fluids, Vol. 5*, Wiley, New York, 1984, pp. 107–126.
6. G. Comini and S. D. Giudice, 'Finite element solution of the incompressible Navier–Stokes equations', *Numer. Heat Transfer*, **5**, 463–478 (1982)
7. A. C. Benim and W. Zinser, 'A segregated formulation of Navier–Stokes equations with finite elements', *Comput. Methods Appl. Mech. Eng.*, **57**, 223–237 (1986).
8. J. C. Rice and R. J. Schnipke, 'An equal-order velocity–pressure formulation that does not exhibit spurious pressure modes', *Comput. Methods. Appl. Mech. Eng.* **58**, 135–149 (1986).
9. P. S. Huyakorn, C. Taylor, R. L. Lee and P. M. Gresho, 'A comparison of various mixed-interpolation finite elements in the velocity–pressure formulation of the Navier–Stokes equations', *Comput. Fluids*, **6**, 25–35 (1978).
10. P. M. Gresho, S. T. Chan, R. L. Lee and C. D. Upson, 'A modified finite element method for solving the time-dependent incompressible Navier–Stokes equations, Part 2. Applications', *Int. j. numer. methods fluids*, **4**, 619–640 (1984).
11. S. V. Patankar, *Numerical Heat Transfer and Fluid Flow*, McGraw-Hill, New York, 1980.
12. M. Bercovier and M. Engelman, 'A finite element for numerical solution of viscous incompressible flows', *J. Comput. Phys.*, **30**, 181–201 (1979).
13. B. Irons and S. Ahmad, *Techniques of Finite Elements*, Wiley, New York, 1980.
14. S.-W. Kim, 'Velocity–pressure integrated versus penalty finite element methods for high Reynolds number flows', *NASA CR-179357*, 1988.
15. S.-W. Kim and C.-P. Chen, 'A multiple-time-scale turbulence model based on variable partitioning of the turbulent kinetic energy spectrum', *AIAA Paper 88-0221*, 1988; also available as *NASA CR-179222*, 1987.
16. S.-W. Kim and Y.-S. Chen, 'A finite element computation of turbulent boundary layer flows with an algebraic stress turbulence model', *Comput. Methods Appl. Mech. Eng.*, **66**, 45–63 (1988); also available as *NASA CR-178967*, 1987.
17. C. E. Thomas, K. Morgan and C. Taylor, 'A finite element analysis of flow over a backward-facing step', *Comput. Fluids*, **9**, 265–278 (1981).
18. G. Dhatt and G. Touzot, *The Finite Element Method Displayed*, translated by G. Cantin, Wiley, New York, 1984.
19. O. R. Burggraf, 'Analytical and numerical studies of the structure of steady separated flows', *J. Fluid Mech.*, **24**, 113–151 (1966).
20. U. Ghia, K. N. Ghia and C. T. Shin, 'High-*Re* solutions for incompressible flow using the Navier–Stokes equations and a multigrid method', *J. Comput. Phys.* **48**, 387–411 (1982).
21. R. Schreiber and H. B. Keller, 'Driven cavity flows by efficient numerical techniques', *J. Comput. Phys.*, **49**, 310–333 (1983).
22. B. F. Armaly, F. Durst, J. C. F. Pereira and B. Schonung, 'Experimental and theoretical investigation of backward-facing step flow', *J. Fluid Mech.*, **127**, 473–496 (1983).
23. J. Kim and P. Moin, 'Application of a fractional-step method to incompressible Navier–Stokes equations', *J. Comput. Phys.*, **59**, 308–323 (1985).
24. S.-W. Kim, 'A critical evaluation of various methods for the analysis of flow–solid interaction in a nest of cylinders subjected to cross-flows', *NASA CR-178996*, 1987, also available as *AIAA Paper 88-3685*.
25. O. C. Zienkiewicz, R. Loehner, K. Morgan and S. Nakazawa, 'Finite elements in fluid mechanics—a decade of progress', in R. H. Gallagher *et al.* (eds), *Finite Elements in Fluids, Vol. 5*, Wiley, New York, 1984, pp. 1–26.
26. S. E. Rogers, U. K. Kaul and D. Kwak, 'A numerical study of three-dimensional incompressible flow around multiple posts', *AIAA Paper 86-0353*, 1986.
27. P. M. Gresho, R. L. Lee and R. L. Sani, 'On the time-dependent solution of the incompressible Navier–Stokes equations in two and three dimensions', in C. Taylor and K. Morgan (eds), *Recent Advances in Numerical Methods in Fluids*, Pineridge Press, Swansea, 1980.